ADVANCES IN ATMOSPHERIC SCIENCES, VOL. 38, SEPTEMBER 2021, 1433–1443

• News & Views •

The First Global Carbon Dioxide Flux Map Derived from TanSat Measurements

Dongxu YANG[1], Yi LIU[1], Liang FENG[2,3], Jing WANG[*1], Lu YAO[1], Zhaonan CAI[1], Sihong ZHU[1], Naimeng LU[4], and Daren LYU[1]

[1]*Institute of Atmospheric Physics*, *Chinese Academy of Sciences*, *Beijing* 100029, *China*

[2]*National Centre for Earth Observation*, *University of Edinburgh*, *Edinburgh*, *EH*9 3*FF*, *UK*

[3]*University of Edinburgh*, *Edinburgh*, *EH*9 3*FF*, *UK*

[4]*National Satellite Meteorological Center*, *China Meteorological Administration Beijing* 100081, *China*

(Received 17 May 2021; accepted 3 June 2021)

ABSTRACT

Space-borne measurements of atmospheric greenhouse gas concentrations provide global observation constraints for top-down estimates of surface carbon flux. Here, the first estimates of the global distribution of carbon surface fluxes inferred from dry-air CO_2 column (XCO_2) measurements by the Chinese Global Carbon Dioxide Monitoring Scientific Experimental Satellite (TanSat) are presented. An ensemble transform Kalman filter (ETKF) data assimilation system coupled with the GEOS-Chem global chemistry transport model is used to optimally fit model simulations with the TanSat XCO_2 observations, which were retrieved using the Institute of Atmospheric Physics Carbon dioxide retrieval Algorithm for Satellite remote sensing (IAPCAS). High posterior error reduction (30%–50%) compared with a priori fluxes indicates that assimilating satellite XCO_2 measurements provides highly effective constraints on global carbon flux estimation. Their impacts are also highlighted by significant spatiotemporal shifts in flux patterns over regions critical to the global carbon budget, such as tropical South America and China. An integrated global land carbon net flux of 6.71 ± 0.76 Gt C yr^{-1} over 12 months (May 2017–April 2018) is estimated from the TanSat XCO_2 data, which is generally consistent with other inversions based on satellite data, such as the JAXA GOSAT and NASA OCO-2 XCO_2 retrievals. However, discrepancies were found in some regional flux estimates, particularly over the Southern Hemisphere, where there may still be uncorrected bias between satellite measurements due to the lack of independent reference observations. The results of this study provide the groundwork for further studies using current or future TanSat XCO_2 data together with other surface-based and space-borne measurements to quantify biosphere–atmosphere carbon exchange.

Key words: TanSat, carbon flux, CO_2, flux inversion

Citation: Yang, D. X., and Coauthors, 2021: The first global carbon dioxide flux map derived from TanSat measurements. *Adv. Atmos. Sci.*, **38**(9), 1433−1443, https://doi.org/10.1007/s00376-021-1179-7.

1. Introduction

Top-down carbon flux inversion by assimilating atmospheric carbon dioxide (CO_2) measurements is a useful tool for evaluating the global carbon budget and was used in the 2019 Refinement to the 2006 Intergovernmental Panel on Climate Change (IPCC) Guidelines for National Greenhouse Gas Inventories. Ground-based measurements provide highly accurate continuous data and have improved our understanding of global carbon flux. However, the sparseness and spatial inhomogeneity of the existing ground-based network limits our ability to infer consistent global- and regional-scale CO_2 sources and sinks (Scholes et al., 2009), especially for tropical and high-latitude regions.

To improve observation coverage, tailor-made satellites have been developed to provide atmospheric greenhouse gas (GHG) measurements at unprecedented precision. The Japanese GHG monitoring satellite mission, Greenhouse Gases Observing Satellite (GOSAT), was launched in 2009 (Kuze et al., 2009), and the U.S. satellite mission, Orbiting Carbon Observatory 2 (OCO-2), was launched in 2014 (Crisp et al., 2017).

* Corresponding author: Jing WANG
Email: jingwang@mail.iap.ac.cn

Satellite measurements are advantageous for constraining top-down flux inversions because they provide continuous global observation coverage. Although satellite measurements are not as accurate as ground-based measurements, the increased spatial coverage can provide additional information not available from sparse surface networks (Buchwitz et al., 2007), and such data have been used in surface carbon flux inversion studies (Peylin et al., 2013; Saeki et al., 2013; Jiang et al., 2016; Chevallier et al., 2019; Wang et al., 2020). The CO_2 column-averaged dry-air mole fractions (XCO_2) measured by GOSAT and OCO-2 have been applied in regional carbon flux optimization studies (Basu et al., 2013; Maksyutov et al., 2013; Feng et al., 2017; Chevallier et al., 2019; Wang et al., 2020).

Recent studies have shown that the accuracy of inversion results inferred from the GOSAT and OCO-2 retrievals is comparable to traditional inversions using accurate but sparse surface networks, indicating that satellite GHG observations provide valuable complementary data for global carbon budget studies (Chevallier et al., 2019; Wang et al., 2020). Assimilation of satellite GHG observations has significantly changed or raised questions about our understanding of spatiotemporal patterns of surface CO_2 fluxes. For example, GOSAT inversion data suggest high European biospheric uptake, nearly twice that suggested by in situ-only studies (Houweling et al., 2015; Feng et al., 2016; Reuter et al., 2017), which would modify the global carbon flux distribution (Houweling et al., 2015). Assimilated GOSAT and OCO-2 XCO_2 measurements have also revealed unexpectedly high net emissions from tropical Africa, which are thought to be mainly caused by substantial land-use change, resulting in the release of carbon from large soil organic carbon stores (Palmer et al., 2019).

The Chinese Global Carbon Dioxide Monitoring Scientific Experimental Satellite (TanSat), funded by the Ministry of Science and Technology of China, the Chinese Academy of Sciences, and the China Meteorological Administration, was launched in December 2016 (Liu and Yang, 2016; Ran et al., 2019). The first global XCO_2 map measured by TanSat was reported in a previous study (Yang et al., 2018), and Total Column Carbon Observing Network validation shows 2.2 ppm accuracy for version 1 of the TanSat L2 data product (Liu et al., 2018). The accuracy and precision of TanSat XCO_2 retrievals were further improved using a wavelength dependence gain factor to correct the spectrum continuum feature (Yang et al., 2020). A new version of TanSat XCO_2 was recently released to the public (Yang et al., 2021), which provides an opportunity to improve our knowledge of global carbon flux from flux inversions based on TanSat measurements.

In this study, we introduce the first estimate of global carbon flux based on TanSat global measurements. The following section shows the TanSat measurements and methods used in the flux inversion. Section 3 introduces the main results of the optimized carbon flux. We then close with our conclusions.

2. Method

2.1. *TanSat measurement*

TanSat flies in a sun-synchronous low Earth orbit (LEO) with an equator crossing time around 1330 local time and operates in three observation modes including nadir (ND), glint (GL), and target modes. ND mode is used when TanSat flies over land surfaces, and GL mode is activated over the ocean to increase the incident signal and ensure the signal-to-noise ratios meet the requirements. The atmospheric carbon dioxide grating spectrometer on board TanSat provides hyperspectral measurements of the O_2 A band (0.76 μm) and CO_2 weak (1.61 μm) and strong (2.04 μm) bands. The ND footprint size of TanSat measurement is ~2 × 2 km with nine footprints across the track in a frame, while the total field-of-view width is ~18 km. The TanSat repeat measurement cycle is 16 days, and the ND and GL measurements are staggered. In ND mode, TanSat has the same ground track interval as OCO-2.

XCO_2 retrieval is performed using the Institute of Atmospheric Physics carbon dioxide retrieval algorithm for satellite remote sensing (Liu et al., 2013; Yang et al., 2015). The version 1 TanSat XCO_2 retrievals only used the CO_2 weak band due to calibration issues on the O_2 A band (which can cause critically biased estimates of surface pressure). Therefore, the flux inversion precision and accuracy were not adequate for studying global surface carbon flux. Further study on solar calibration measurements revealed a remaining feature on the solar spectrum fitting residual. A Fourier series model was applied as a gain factor to the continuum in the retrieval, significantly improving the fitting residual, especially on the O_2 A band. The O_2 A band and CO_2 weak band measurements have been used together in new retrievals that correct the parameters of water vapor, surface pressure, temperature, aerosol, cirrus, and instrument model. A genetic algorithm was used in post screening, and then a multiple linear regression model was applied to correct bias (Yang et al., 2020). In this study, we used a 15-month (March 2017–May 2018) XCO_2 retrieval from TanSat ND measurements.

Only "good" retrievals have been provided in the TanSat v2 product used in flux inversion. We used single sounding uncertainty (posterior error) to construct weighted time–space average data (Crowell et al., 2019). First, we calculated a 1-second span average:

$$\overline{X_{CO_2,1s}} = \sum_{i=1}^{N} \left(X_{CO_2,i} \sigma_i^{-2} \right) \Big/ \sum_{i=1}^{N} \sigma_i^{-2} , \tag{1}$$

where $X_{CO_2,i}$ is the ith sounding value in a 1-second span with a total of N soundings, and σ_i is the corresponding posterior error. The summary includes all soundings in a 1-second span, and the uncertainty for the 1-second average is:

$$\overline{\sigma_{1s,\sigma}} = 1\Big/\sqrt{N\sum_{i=1}^{N}\sigma_i^{-2}}\,, \tag{2}$$

where we assumed soundings in a 1-second span were highly correlated. Because the posterior error mainly considered the theoretical error from the measurement noise level, the $\overline{\sigma_{1s,\sigma}}$ estimation was sometimes lower than real measurement uncertainty. Therefore, we also considered the standard deviation $\overline{\sigma_{1s,std}}$; the uncertainty of a 1-second span, $\overline{\sigma_{1s}}$, was the maximum of either $\overline{\sigma_{1s,\sigma}}$ or $\overline{\sigma_{1s,std}}$. This differs from the 1-second spans of OCO-2 because TanSat L2 sounding values have not been corrected for the bias of small areas. Thus, small systematic uncertainty, such as floor error, was not considered.

In this study, we used a 5-second span average for flux inversion. The $\overline{X_{CO_2,5s}}$ and $\overline{\sigma_{5s}}$ values were constructed using the methods for 1-second spans of sounding measurements.

2.2. *Carbon flux inversion system*

We used an ensemble transform Kalman filter (ETKF) data assimilation system (Feng et al., 2009, 2011, 2016) to estimate global and regional carbon flux. The carbon flux and CO_2 concentration were optimized by TanSat XCO_2 measurements via:

$$\boldsymbol{x}^{a} = \boldsymbol{x}^{f} + \boldsymbol{K}\cdot\left[\boldsymbol{y}_{obs} - H_{oo}\left(\boldsymbol{x}^{f}\right)\right], \tag{3}$$

where $\boldsymbol{x}^{a}$ and $\boldsymbol{x}^{f}$ are the a posteriori and a priori fluxes, respectively. H_{oo} is the observation operator that describes the relationship between the state vector and the observations. $\boldsymbol{y}_{obs}$ is XCO_2 measured by TanSat, and $\boldsymbol{K}$ is the Kalman gain matrix, which determines the adjustment to the a priori based on the difference between the model and observations and their uncertainties as follows:

$$\boldsymbol{K} = \boldsymbol{P}^{f}\cdot\boldsymbol{H}^{T}\cdot\left[\boldsymbol{H}\cdot\boldsymbol{P}^{f}\cdot\boldsymbol{H}^{T} + \boldsymbol{R}\right]^{-1}, \tag{4}$$

where $\boldsymbol{R}$ is the observation error covariance matrix, namely, a diagonal matrix representing measurement errors, including instrument error, retrieval error, model error, and representation error (Peylin et al., 2002). $\boldsymbol{P}^{f}$ is the a priori error covariance matrix. The Jacobian of the observation operator, $\boldsymbol{H}$, maps $\boldsymbol{P}^{f}$ into observation space. In our carbon flux inversion system, we used the chemistry transport model (CTM) GEOS-Chem (v9-02) in forward simulation $[H\left(\boldsymbol{x}^{f}\right)]$ and performed an ensemble run to establish the connection between surface fluxes and atmospheric CO_2 concentrations ($\boldsymbol{H}$).

We used sequentially assimilated TanSat 5-second averaged measurements day by day in each assimilation step (1 month) to optimize the a priori estimation of surface CO_2 fluxes. The GEOS-5 meteorological analyses, provided by the NASA Goddard Global Modelling and Assimilation Office, were used to drive the GEOS-Chem run. The model was run at a horizontal resolution of 4° (latitude) × 5° (longitude) with 47 vertical levels, which spanned from the surface to the mesosphere, typically with 35 levels in the troposphere. Monthly inventories have been used as the a priori flux for GEOS-Chem runs, including ocean flux (Takahashi et al., 2009), biomass burning fluxes (van der Werf et al., 2010), 3-hourly terrestrial biosphere fluxes (Olsen, 2004), and fossil fuel emissions (Oda and Maksyutov, 2011). For the terrestrial biosphere, we used a 3-hour flux to better represent and optimize the uptakes and emissions from photosynthesis and respiration processes, respectively (Olsen, 2004). The inversion for surface flux spanned 792 regions globally, including 475 land regions and 317 ocean regions, based on a TransCom 3 study (Gurney et al., 2002).

3. Results

3.1. *Annually integrated global carbon net flux*

In this study, only the ND model land observations were applied to constrain the flux optimization. Due to the low signal-to-noise ratio, the ND measurements over the ocean are not provided in the L2 XCO_2 data product, and no further information is provided by TanSat ocean measurements. Therefore, a very strong prior constraint was applied to the ocean CO_2 flux. The inversion result is shown as carbon flux based on CO_2 flux using the mass ratio between CO_2 and carbon.

Error reduction for global carbon sinks indicates how well the measurements optimized the estimations. The error reduction in July was greater than in other months (Fig. 1); for example, it was > 50% in northern Asia, Europe, and America, but lower in Australia, southern Asia, and India. South America and Africa showed 20%–40% error reduction. TanSat measurements improved results in South Africa mostly in April and October, in North and South America mostly in July, and in

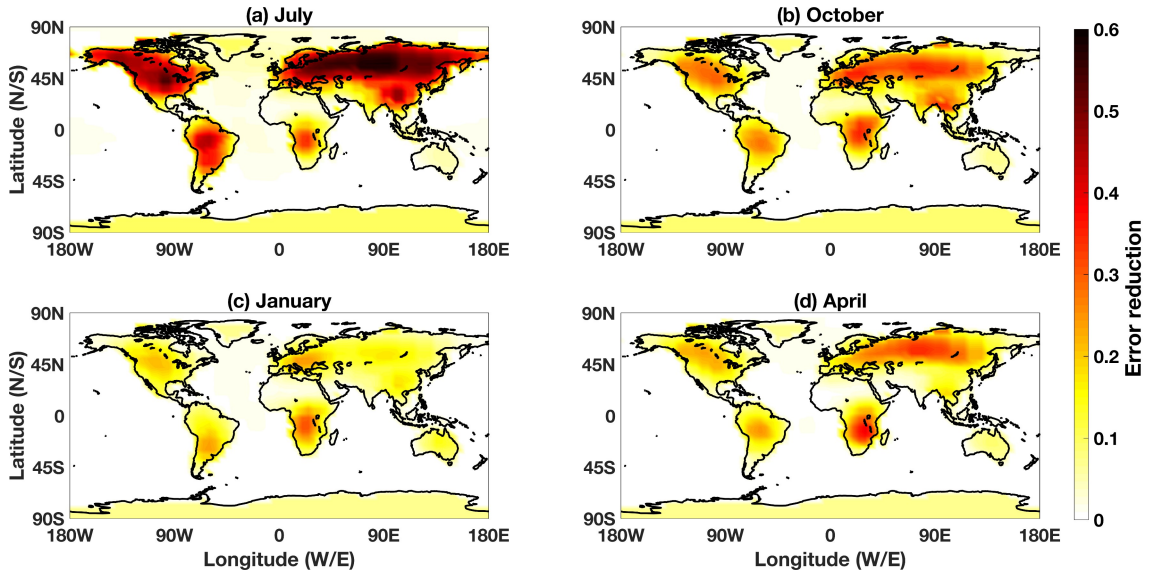

Fig. 1. The reductions in uncertainty for (a) July 2017, (b) October 2017, (c) January 2018, and (d) April 2018.

northern Eurasia in all three months.

The global annual carbon sinks (Fig. 2) constrained by TanSat measurements differed significantly from a priori fluxes. For example, the land sink increased in most of Northern Asia, Europe, and the Americas, but decreased in the middle of Africa and India. Similar results have been reported in GOSAT and OCO-2 CO_2 flux inversion studies (Wang et al., 2019, 2020). The land sink also increased in southwest China, which is consistent with carbon flux estimations based on additional ground-based in-situ measurements from Asia (Wang et al., 2020). The optimization was not significant over the ocean because no direct measurements were used to constrain the oceanic carbon flux.

Our TanSat inversion indicated a land net flux integrated over 12 months (May 2017–April 2018) of 6.71 Gt C yr^{-1} with an uncertainty of 0.76 Gt C yr^{-1}. Table 1 shows the land carbon net flux over the same period constrained by the new L2 OCO-2 XCO2 data product (v10) as a reference. The annul integrated OCO-2 net carbon flux was 5.13 ± 0.59 Gt C yr^{-1}, which is 23.5% lower than the TanSat results. Several studies have reported different carbon flux estimations based on satellite measurements for 2009 onwards. The GOSAT measurement was the first spaced-based GHG measurement used in global CO_2 flux estimation (Basu et al., 2013). GOSAT measurements indicated land net carbon fluxes estimated by the carbon tracker (Peters et al., 2007; https://www.esrl.noaa.gov/gmd/ccgg/carbontracker/) of 7.86 ± 1.26 Gt C yr^{-1} in 2017 and 7.61 ± 1.78 Gt C yr^{-1} in 2018. The OCO-2 model intercomparison project showed 10 inversion model parallel studies with results ranging from 5.75 to 8.97 Gt C yr^{-1} from June 2017 to May 2018.

3.2. *Seasonal and regional CO_2 flux*

Seasonal net carbon flux was grouped every three months and denoted following the Northern Hemisphere seasons, namely, summer (June, July, August), autumn (September, October, November), winter (December, January, February), and spring (March, April, May). The distribution of global carbon flux differed significantly from a priori flux after assimilation of TanSat measurements (Fig. 3). For example, the measurements (satellite data) significantly changed carbon fluxes for South America for the whole year (Fig. 4). The South America tropical region showed the largest impacts from TanSat measurements, with the seasonal phase shifted significantly from a priori fluxes. We found that the satellite did not provide dense measurements over tropical South America, but even a small amount of TanSat data can still significantly change the carbon flux feature. TanSat measurements increased carbon sinks in spring and summer around Eurasia, including in Europe and boreal and temperate Eurasia, compared with a priori fluxes. North Africa also showed significant increases in the carbon sink in winter. In addition, the seasonal variation of India decreased during spring and summer.

We also observed changes in China's carbon flux in autumn, winter, and spring; in general, the carbon sink increased compared to a priori fluxes, especially in southwest China in the summer and autumn. Similar results have been reported by studies of vegetation trend measurements (Chen et al., 2019) and flux estimations (Wang et al., 2020).

Figure 5 shows regional carbon flux from OCO-2 and TanSat measurements, as well as a priori fluxes. OCO-2 and TanSat have similar optimization effects on a priori fluxes in most regions. The biggest discrepancy was in the Southern Hemisphere, where TanSat measurements and a priori fluxes indicated a source, whereas OCO-2 measurements indicated a sink; the difference in outcomes was driven in large part by results from tropical and temperate South America. This contradiction has also been reported when comparing results from GOSAT and OCO-2 measurements (Wang et al., 2019).

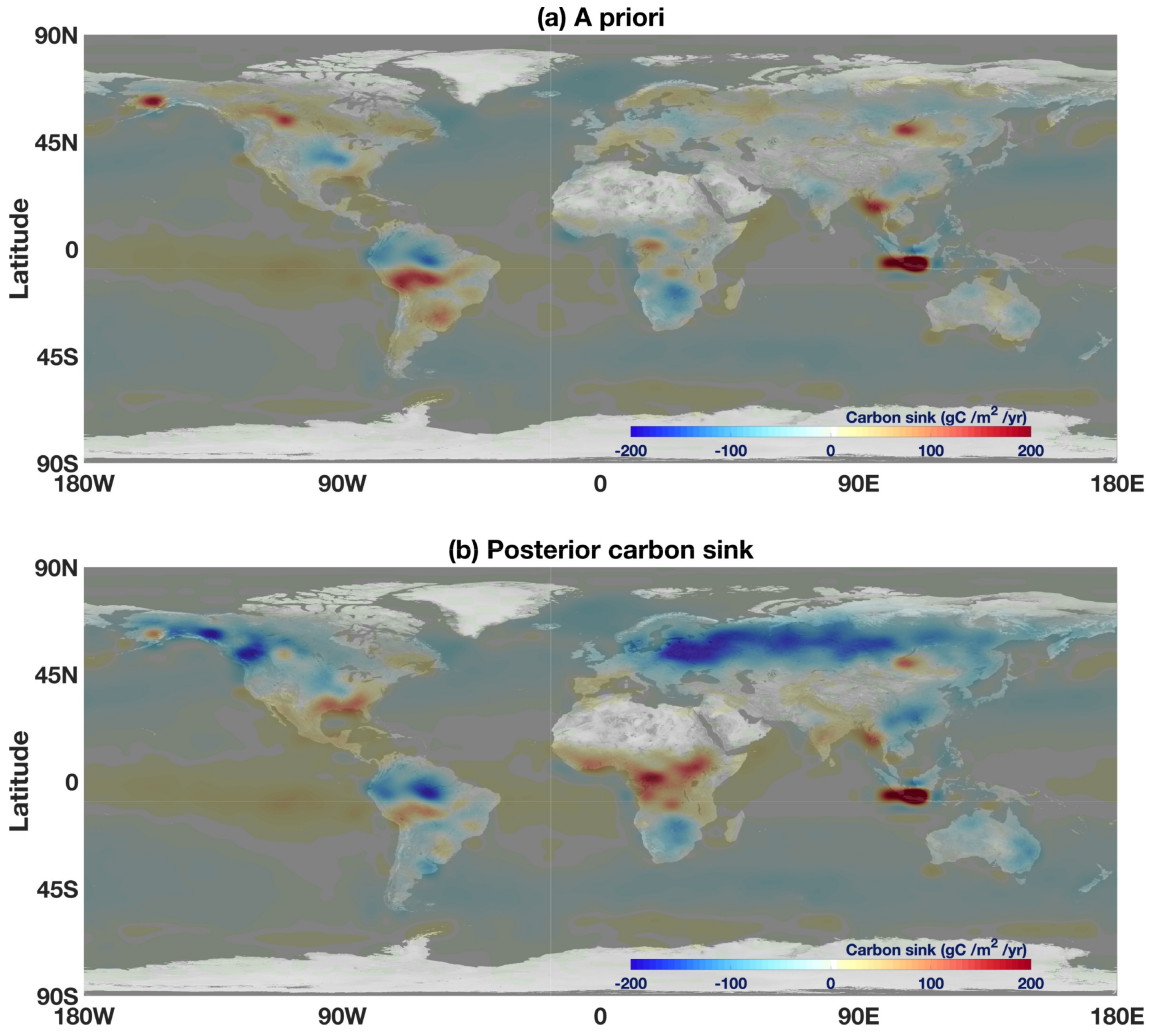

Fig. 2. The annual carbon sink optimized by GOSAT measurements (b) from a priori estimates (a). The color bar indicates the carbon sink.

Table 1. The a priori and a posteriori fluxes estimated by TanSat (v2) and OCO-2 (v10) for 11 TransCom regions and continents.

	A priori		TanSat		OCO-2	
Region	Flux	1-σ	Flux	1-σ	Flux	1-σ
North American Boreal (NAB)	0.17	0.33	−0.82	0.19	−0.23	0.19
North American Temperate (NAT)	1.52	0.58	1.53	0.29	1.62	0.27
South American Tropical (SAT)	0.094	0.40	0.78	0.26	0.09	0.22
South American Temperate (SAM)	0.49	0.39	0.065	0.26	−0.76	0.20
North Africa (NAF)	0.20	0.24	1.059	0.18	0.81	0.15
South Africa (SAF)	−0.057	0.44	0.74	0.25	−0.19	0.18
Eurasia Boreal (EAB)	0.10	0.60	−1.12	0.23	−0.12	0.25
Eurasia Temperate (EAT)	3.83	0.42	3.68	0.24	2.89	0.22
Tropical Asia (TA)	1.23	0.27	0.90	0.20	0.61	0.16
Australia (AUS)	0.069	0.20	−0.21	0.17	−0.056	0.15
Europe (EU)	1.15	0.66	−0.18	0.30	0.18	0.28
North land (NL)	6.78	1.43	3.10	0.52	4.34	0.41
South land (SL)	0.50	0.62	0.60	0.38	−1.00	0.30
Tropical land (TL)	1.52	0.54	2.73	0.36	1.51	0.30
Global Land	9.08	1.74	6.71	0.77	5.13	0.59

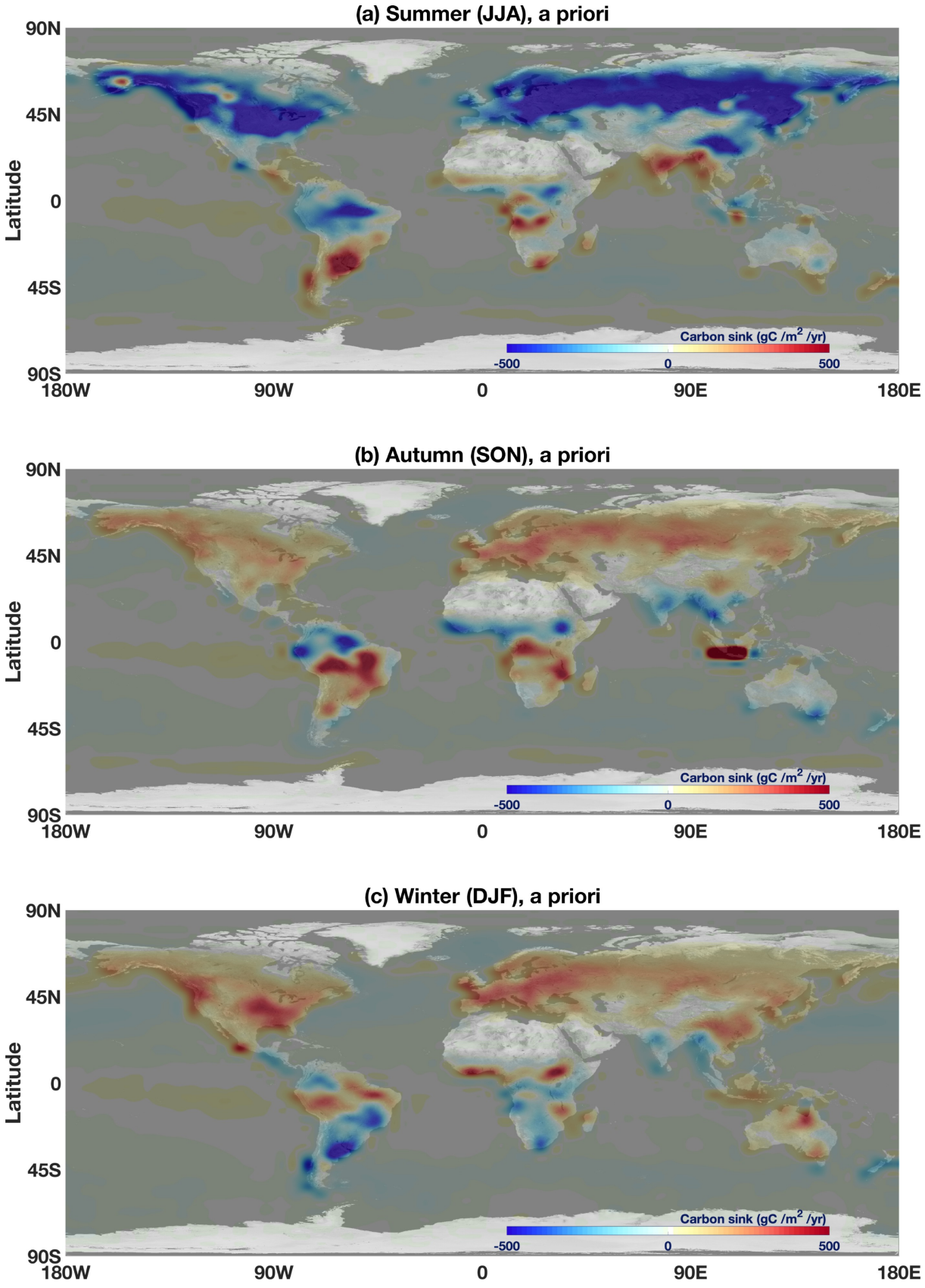

Fig. 3. The a priori (upper row) and a posteriori (lower row) seasonal carbon sinks constrained by TanSat measurements. The columns indicate summer, autumn, winter, and spring from left to right.

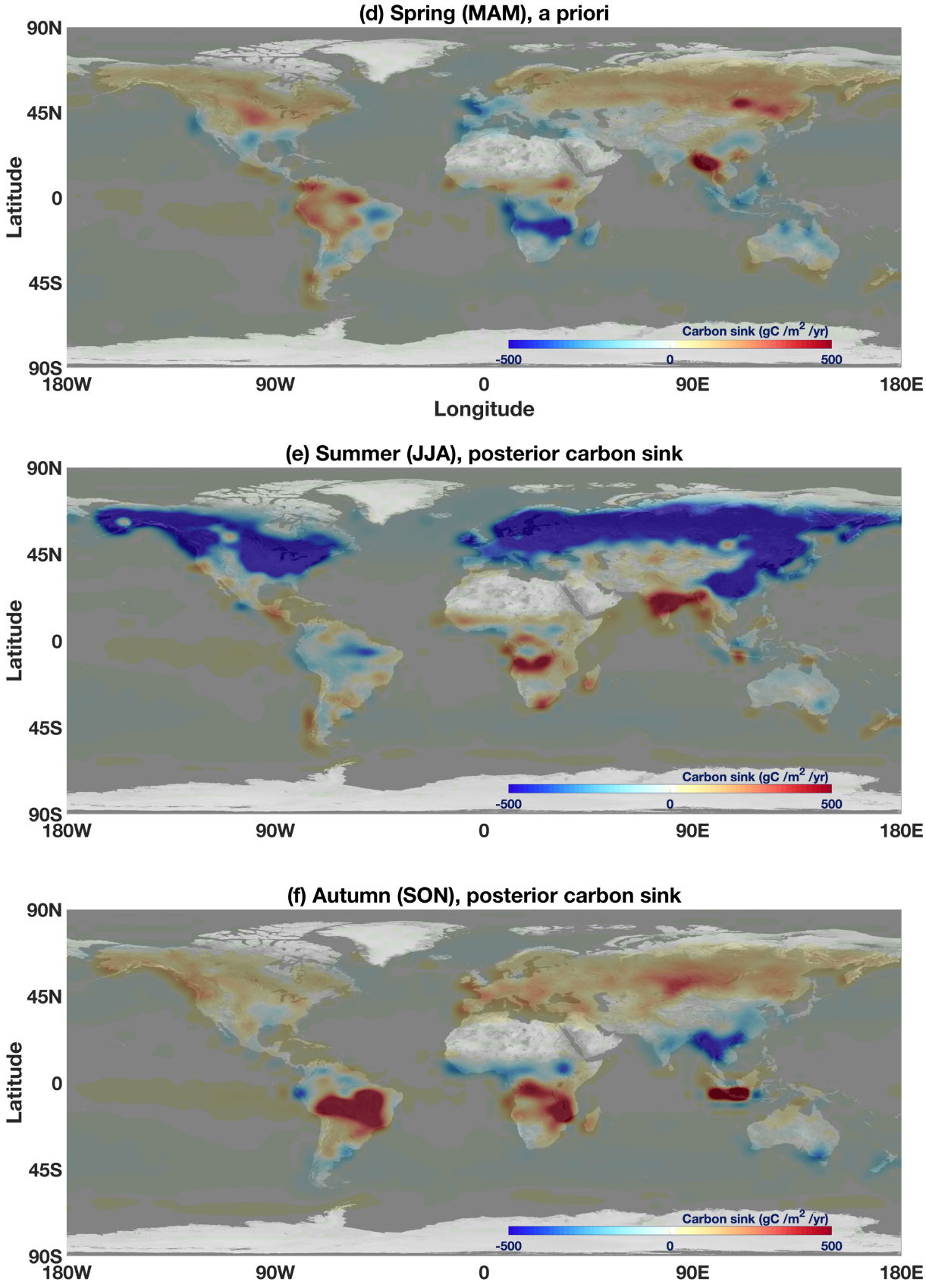

Fig. 3. (Continued).

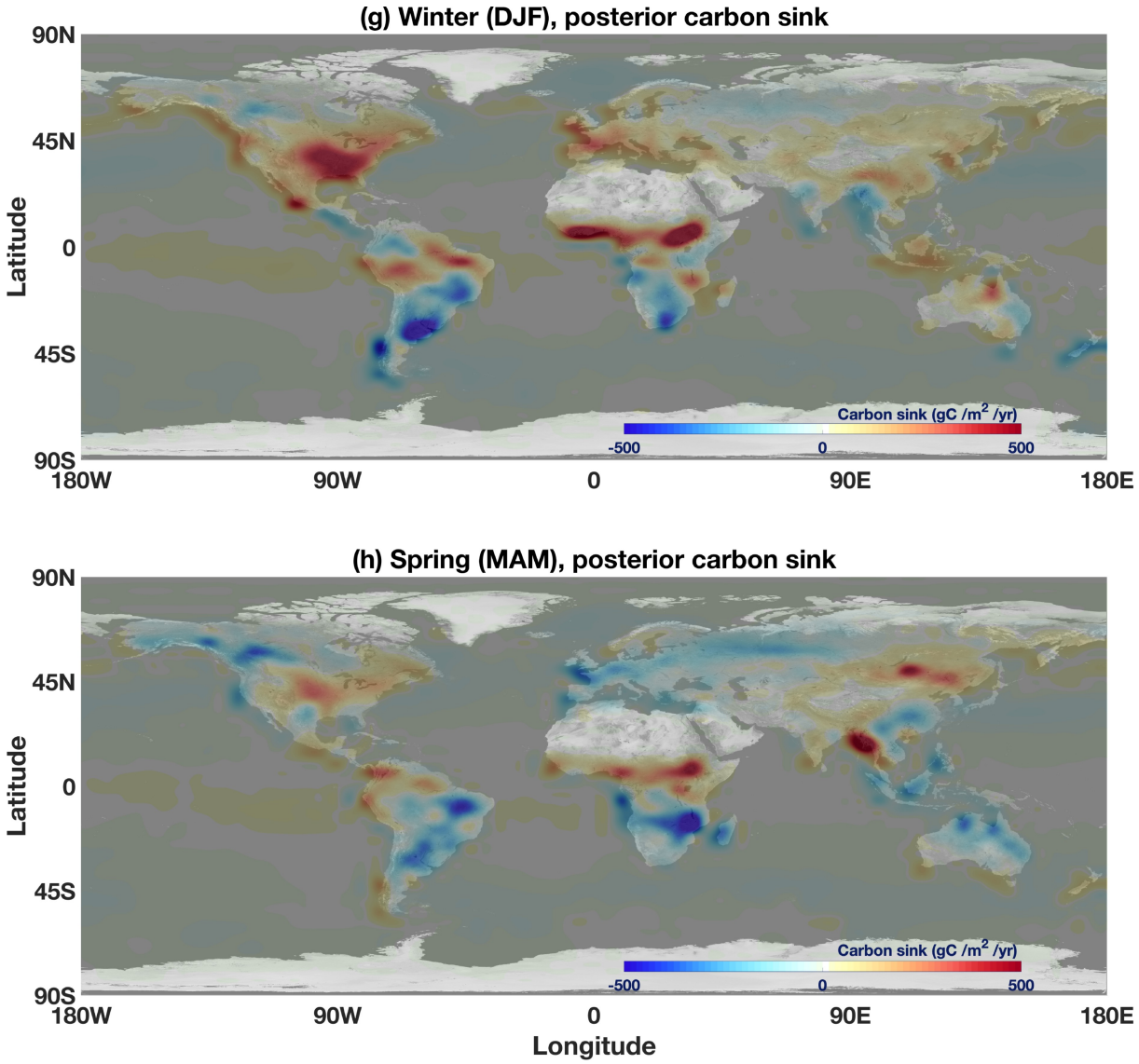

Fig. 3. (Continued).

4. Conclusions and outlook

We described the first attempt at estimating global carbon flux using TanSat XCO_2 measurements. We used an ETKF data assimilation system coupled with the GEOS-Chem CTM in a top-down carbon flux inversion. The error reduction compared to a priori estimates demonstrated the impact of assimilating global satellite XCO_2 measurements, which resulted in significant changes in spatiotemporal flux patterns throughout the year from May 2017 to April 2018. Our TanSat inversion indicated an annual integrated global land carbon net flux of 6.71 ± 0.76 Gt C yr^{-1}, compared to annual totals of 5.75–8.97 Gt C yr^{-1} for inversions based on OCO-2 XCO_2 data.

These carbon flux data are publicly accessible worldwide on the China GEO TanSat data service archive, the Cooperation on the Analysis of Carbon Satellites Data (CASA; www.chinageoss.org/tansat), which is hosted by the International Reanalysis Cooperation on Carbon Satellites Data (IRCSD).

TanSat provides preliminary global measurements that extend the ground-based network from local measurements to global estimates. However, the coverage, repeat, pixel size, and accuracy of measurements are still inadequate to meet the Global Stocktake of the Paris Agreement and inventory validation requirements of IPCC standards. For example, GOSAT measurements have indicated that flux estimation is sensitive to measurement coverage (Deng et al., 2014). XCO_2 measurements are also sensitive to regional flux inversion (Feng et al., 2009; Palmer et al., 2011). The future European Copernicus Carbon Dioxide Monitoring satellite mission (Kuhlmann et al., 2019) will improve measurements of global coverage and investigations of anthropogenic emissions. The plan for the next TanSat mission has been discussed and is in the design phase. One possibility is a multi-satellite LEO constellation. Several satellites would capture global background measure-

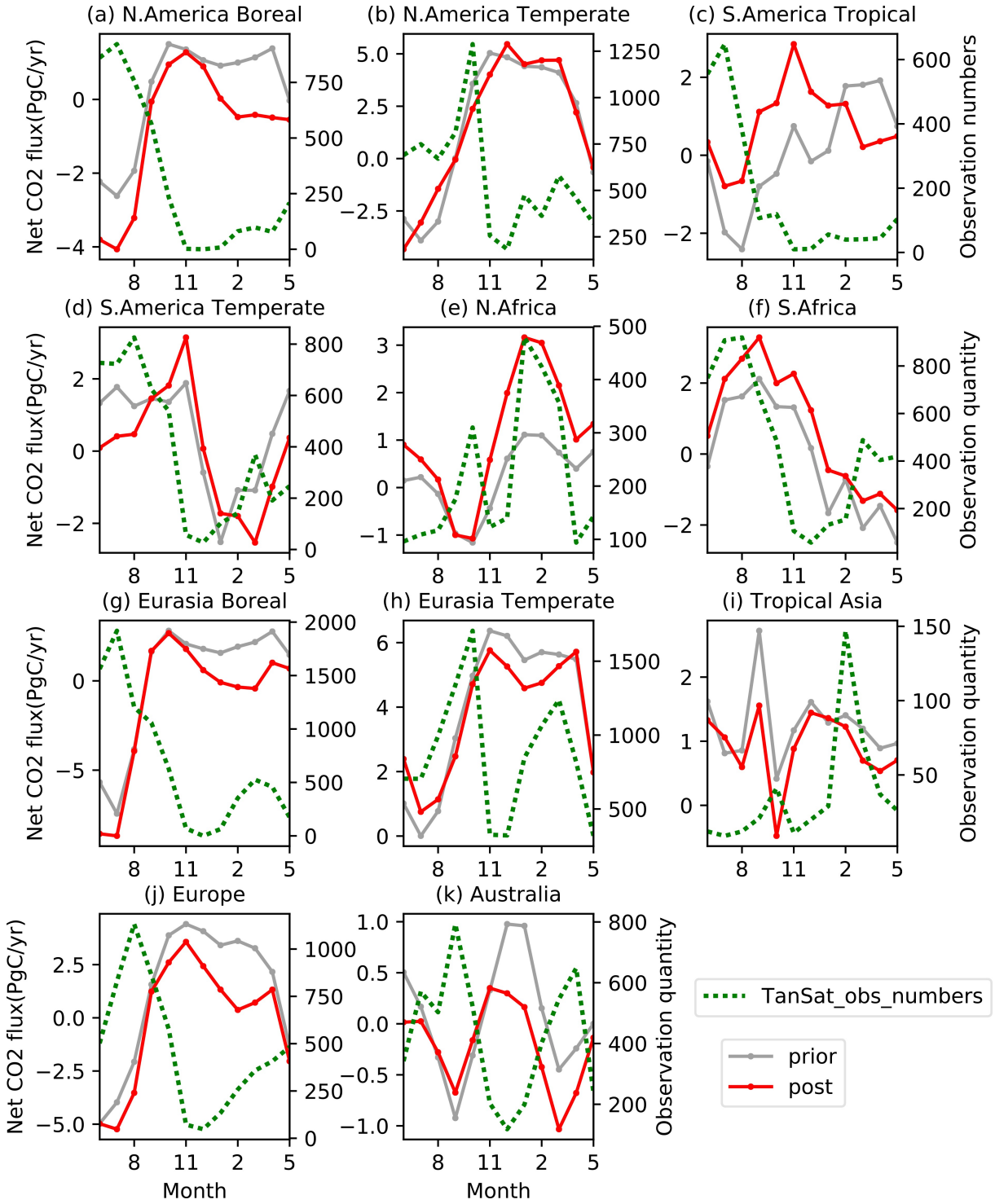

Fig. 4. The a priori and a posteriori CO_2 flux trends for 11 TransCom land regions shown with measurement quantities. The names at the top of each subplot indicate regions.

ments with large pixel size and a wide swath, while others would focus on target measurements for city and point sources with a small pixel size. This would capture carbon sinks and sources at multiple scales to elucidate the influences of natural processes and anthropogenic activities on the carbon cycle.

Column CO_2 measurements are still inadequate for separating local carbon exchanges from long-range transport processes because the signal is mixed into the column value (Keppel-Aleks et al., 2011). The signal of local flux is critical to city and point-source research. Ground-based measurements near the surface will be helpful for future investigations. Therefore, coordinating satellites and surface measurement networks will significantly improve the study of small-scale anthropo-

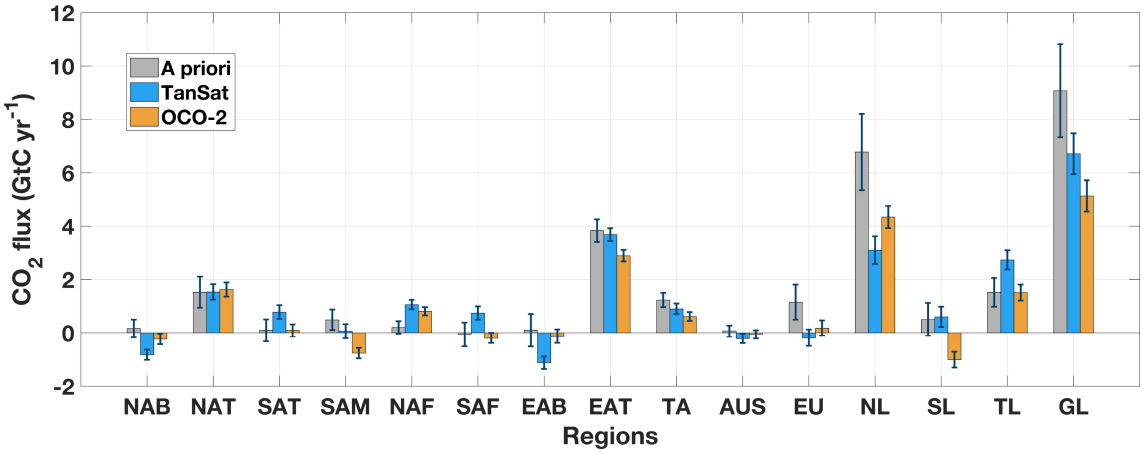

Fig. 5. The carbon flux estimated by TanSat and OCO-2 measurements and the a priori flux in 11 TransCom land regions, South Land (SL), North Land (NL), and globally.

genic emission sources.

Acknowledgements. This work is supported by the National Key R&D Program of China (Grant No. 2016YFA0600203), the Key Research Program of the Chinese Academy of Sciences (ZDRW-ZS-2019-1), the National Key R&D Program of China (Grant No. 2017YFB0504000), and the Youth Program of the National Natural Science Foundation of China (Grant No. 41905029). Liang FENG is supported by the UK NERC National Centre for Earth Observation (NCEO). The TanSat L1B data service is provided by IRCSD and CASA (131211KYSB20180002). We also thank the FENGYUN Satellite Data Center of the National Satellite Meteorological Center, who provided the TanSat L1B data service. The authors thank the TanSat mission and highly appreciate the support from everyone involved.

REFERENCES

Basu, S., and Coauthors, 2013: Global CO_2 fluxes estimated from GOSAT retrievals of total column CO_2. *Atmospheric Chemistry and Physics*, **13**, 8695–8717, https://doi.org/10.5194/acp-13-8695-2013.

Buchwitz, M., O. Schneising, J. P. Burrows, H. Bovensmann, M. Reuter, and J. Notholt, 2007: First direct observation of the atmospheric CO_2 year-to-year increase from space. *Atmospheric Chemistry and Physics*, **7**, 4249–4256, https://doi.org/10.5194/acp-7-4249-2007.

Chen, C., and Coauthors, 2019: China and India lead in greening of the world through land-use management. *Nature Sustainability*, **2**, 122–129, https://doi.org/10.1038/s41893-019-0220-7.

Chevallier, F., M. Remaud, C. W. O'Dell, D. Baker, P. Peylin, and A. Cozic, 2019: Objective evaluation of surface- and satellite- driven carbon dioxide atmospheric inversions. *Atmos. Chem. Phys.*, **19**, 14233–14251, https://doi.org/10.5194/acp-19-14233-2019.

Crisp, D., and Coauthors, 2017: The on-orbit performance of the Orbiting Carbon Observatory-2 (OCO-2) instrument and its radiometrically calibrated products. *Atmospheric Measurement Techniques*, **10**, 59–81, https://doi.org/10.5194/amt-10-59-2017.

Crowell, S., and Coauthors, 2019: The 2015-2016 carbon cycle as seen from OCO-2 and the global in situ network. *Atmospheric Chemistry and Physics*, **19**, 9797–9831, https://doi.org/10.5194/acp-19-9797-2019.

Deng, F., and Coauthors, 2014: Inferring regional sources and sinks of atmospheric CO_2 from GOSAT XCO_2 data. *Atmospheric Chemistry and Physics*, **14**, 3703–3727, https://doi.org/10.5194/acp-14-3703-2014.

Feng, L., P. I. Palmer, H. Bösch, and S. Dance, 2009: Estimating surface CO_2 fluxes from space-borne CO_2 dry air mole fraction observations using an ensemble Kalman Filter. *Atmospheric Chemistry and Physics*, **9**, 2619–2633, https://doi.org/10.5194/acp-9-2619-2009.

Feng, L., P. I. Palmer, Y. Yang, R. M. Yantosca, S. R. Kawa, J.-D. Paris, H. Matsueda, and T. Machida, 2011: Evaluating a 3-D transport model of atmospheric CO_2 using ground-based, aircraft, and space-borne data. *Atmospheric Chemistry and Physics*, **11**, 2789–2803, https://doi.org/10.5194/acp-11-2789-2011.

Feng, L., P. I. Palmer, R. J. Parker, N. M. Deutscher, D. G. Feist, R. Kivi, I. Morino, and R. Sussmann, 2016: Estimates of European uptake of CO2 inferred from GOSAT XCO2 retrievals: Sensitivity to measurement bias inside and outside Europe. *Atmos. Chem. Phys.*, **16**, 1289–1302, https://doi.org/10.5194/acp-16-1289-2016.

Feng, L., and Coauthors, 2017: Consistent regional fluxes of CH_4 and CO_2 inferred from GOSAT proxy XCH_4: XCO_2 retrievals, 2010-2014. *Atmospheric Chemistry and Physics*, **17**, 4781–4797, https://doi.org/10.5194/acp-17-4781-2017.

Gurney, K. R., and Coauthors, 2002: Towards robust regional estimates of CO_2 sources and sinks using atmospheric transport models. *Nature*, **415**, 626–630, https://doi.org/10.1038/415626a.

Houweling, S., and Coauthors, 2015: An intercomparison of inverse models for estimating sources and sinks of CO_2 using GOSAT measurements. *J. Geophys. Res.*, **120**, 5253–5266, https://doi.org/10.1002/2014JD022962.

Jiang, F., and Coauthors, 2016: A comprehensive estimate of recent carbon sinks in China using both top-down and bottom-up approaches. *Sci. Rep.*, **6**, 22130, https://doi.org/10.1038/srep22130.

Keppel-Aleks, G., P. O. Wennberg, and T. Schneider, 2011: Sources of variations in total column carbon dioxide. *Atmospheric Chemistry and Physics*, **11**, 3581–3593, https://doi.org/10.5194/acp-11-3581-2011.

Kuhlmann, G., G. Broquet, J. Marshall, V. Clément, A. Löscher, Y. Meijer, and D. Brunner, 2019: Detectability of CO_2 emission plumes of cities and power plants with the Copernicus Anthropogenic CO_2 Monitoring (CO2M) mission. *Atmospheric Measurement Techniques*, **12**, 6695–6719, https://doi.org/10.5194/amt-12-6695-2019.

Kuze, A., H. Suto, M. Nakajima, and T. Hamazaki, 2009: Thermal and near infrared sensor for carbon observation Fourier-transform spectrometer on the Greenhouse Gases Observing Satellite for greenhouse gases monitoring. *Appl. Opt.*, **48**, 6716–6733, https://doi.org/10.1364/AO.48.006716.

Liu, Y., D. X. Yang, and Z. N. Cai, 2013: A retrieval algorithm for TanSat XCO_2 observation: Retrieval experiments using GOSAT data. *Chinese Science Bulletin*, **58**, 1520–1523, https://doi.org/10.1007/s11434-013-5680-y.

Liu, Y., and D. X. Yang, 2016: Advancements in theory of GHG observation from space. *Science Bulletin*, **61**(5), 349–352, https://doi.org/10.1007/s11434-016-1022-1.

Liu, Y., and Coauthors, 2018: The TanSat mission: Preliminary global observations. *Science Bulletin*, **63**(18), 1200–1207, https://doi.org/10.1016/j.scib.2018.08.004.

Maksyutov, S., and Coauthors, 2013: Regional CO_2 flux estimates for 2009–2010 based on GOSAT and ground-based CO_2 observations. *Atmospheric Chemistry and Physics*, **13**, 9351–9373, https://doi.org/10.5194/acp-13-9351-2013.

Oda, T., and S. Maksyutov, 2011: A very high-resolution (1 km×1 km) global fossil fuel CO_2 emission inventory derived using a point source database and satellite observations of nighttime lights. *Atmospheric Chemistry and Physics*, **11**, 543–556, https://doi.org/10.5194/acp-11-543-2011.

Olsen, S. C., 2004: Differences between surface and column atmospheric CO_2 and implications for carbon cycle research. *J. Geophys. Res.*, **109**, D02301, https://doi.org/10.1029/2003JD003968.

Palmer, P., L. Feng, and H. Boesch, 2011: Spatial resolution of tropical terrestrial CO2 fluxes inferred using space-borne column CO2 sampled in different earth orbits: The role of spatial error correlations. *Atmospheric Measurement Techniques*, **4**(9), 1995–2006, https://doi.org/10.5194/amt-4-1995-2011.

Palmer, P. I., L. Feng, D. Baker, F. Chevallier, H. Bösch, and P. Somkuti, 2019: Net carbon emissions from African biosphere dominate pan-tropical atmospheric CO_2 signal. *Nature Communications*, **10**, 3344, https://doi.org/10.1038/s41467-019-11097-w.

Peters, W., and Coauthors, 2007: An atmospheric perspective on North American carbon dioxide exchange: CarbonTracker. *Proceedings of the National Academy of Sciences of the United States of America*, **104**(48), 18 925–18 930, https://doi.org/10.1073/pnas.0708986104.

Peylin, P., D. Baker, J. Sarmiento, P. Ciais, and P. Bousquet, 2002: Influence of transport uncertainty on annual mean and seasonal inversions of atmospheric CO_2 data. *J. Geophys. Res.*, **107**(D19), 4385, https://doi.org/10.1029/2001JD000857.

Peylin, P., and Coauthors, 2013: Global atmospheric carbon budget: Results from an ensemble of atmospheric CO_2 inversions. *Biogeosciences*, **10**, 6699–6720, https://doi.org/10.5194/bg-10-6699-2013.

Ran, Y., and X. Li, 2019: TanSat: A new star in global carbon monitoring from China. *Scientific Bulletin*, **64**(5), 284–285, https://doi.org/10.1016/j.scib.2019.01.019.

Reuter, M., and Coauthors, 2017: How much CO_2 is taken up by the European terrestrial biosphere? *Bull. Amer. Meteor. Soc.*, **98**, 665–671, https://doi.org/10.1175/BAMS-D-15-00310.1.

Saeki, T., and Coauthors, 2013: Inverse modeling of CO_2 fluxes using GOSAT data and multi-year ground-based observations. *SOLA*, **9**, 45–50, https://doi.org/10.2151/sola.2013-011.

Scholes, R. J., P. M. S. Monteiro, C. L. Sabine, and J. G. Canadell, 2009: Systematic long-term observations of the global carbon cycle. *Trends in Ecology & Evolution*, **24**, 427–430, https://doi.org/10.1016/j.tree.2009.03.006.

Takahashi, T., and Coauthors, 2009: Corrigendum to "Climatological mean and decadal change in surface ocean PCO_2, and net sea-air CO_2 flux over the global oceans" [Deep Sea Res. II 56 (2009) 554–577]. *Deep Sea Research Part I: Oceanographic Research Papers*, **56**, 2075–2076, https://doi.org/10.1016/j.dsr.2009.07.007.

van der Werf, G. R., and Coauthors, 2010: Global fire emissions and the contribution of deforestation, savanna, forest, agricultural, and peat fires (1997–2009). *Atmospheric Chemistry and Physics*, **10**, 11 707–11 735, https://doi.org/10.5194/acp-10-11707-2010.

Wang, H., F. Jiang, J. Wang, W. Ju, and J. M. Chen, 2019: Terrestrial ecosystem carbon flux estimated using GOSAT and OCO-2 XCO_2 retrievals. *Atmos. Chem. Phys.*, **19**, 12067–12082, https://doi.org/10.5194/acp-19-12067-2019.

Wang, J., and Coauthors, 2020: Large Chinese land carbon sink estimated from atmospheric carbon dioxide data. *Nature*, **586**, 720–723, https://doi.org/10.1038/s41586-020-2849-9.

Yang, D. X., Y. Liu, Z. N. Cai, J. B. Deng, J. Wang, and X. Chen, 2015: An advanced carbon dioxide retrieval algorithm for satellite measurements and its application to GOSAT observations. *Science Bulletin*, **60**(23), 2063–2066, https://doi.org/10.1007/s11434-015-0953-2.

Yang, D. X., Y. Liu, Z. N. Cai, X. Chen, L. Yao, and D. R. Lu, 2018: First global carbon dioxide maps produced from TanSat measurements. *Advances in Atmospheric Sciences*, **35**, 621–623, https://doi.org/10.1007/s00376-018-7312-6.

Yang, D. X., and Coauthors, 2020: Toward high precision XCO_2 retrievals from TanSat observations: Retrieval improvement and validation against TCCON measurements. *J. Geophys. Res.*, **125**, e2020JD032794, https://doi.org/10.1029/2020JD032794.

Yang, D. X., and Coauthors, 2021: A new TanSat XCO_2 global product towards climate studies. *Advances in Atmospheric Sciences*, **38**(1), 8–11, https://doi.org/10.1007/s00376-020-0297-y.